





Finite Element Analysis of Voided Reinforced Concrete Slabs Enhanced by GFRP Sheets under Monotonic and Repeated Loads

Shahad H. Mtashar ^{1,*}, Adel A. Al-Azzawi ²

¹Ministry of Construction and Housing and Municipalities and Public Work, Baghdad, Iraq

²Department of Civil Engineering, Al-Nahrain University, Baghdad, Iraq

ABSTRACT

Six (1000*1000 mm²) slab specimens were cast and tested as two-way simply supported slabs previously (three under monotonic loading and three under repeated loading) are used in this research. The tested specimens consist of one solid slab and two voided slabs with the following variables (type of slab (solid and voided), presence of steel fibers (0% and 1%), and the presence of GFRP layers). This paper presents the results of tested slabs and the 3D-Nonlinear finite element (ABAQUS program) is proposed to verify the tested slabs under monotonic and repeated loading. The process of modeling the structure components of the tested slabs will be discussed in detail, including the creation of the parts, model material properties, surface interaction, loading method, boundary conditions, and meshing. Then, the experimental findings will be compared to the proposed FE models. A parametric study with new variables has been investigated that affect the behavior of reinforced concrete slabs and is not implemented in the experimental part of this study. These specimens are divided into two groups according to the nature of loading as in the experimental work. The created finite element models can accurately reflect the test results with an acceptable degree of difference in deflection and ultimate load by 10%. The crack patterns obtained using finite element models for the investigated specimens under monotonic and repeated loading are extremely similar to the crack patterns observed in the experimental work.

Keywords: Finite element, Monotonic loading, Repeated loading, Two-way voided slab, GFRP, ABAQUS

1. INTRODUCTION

The member used in the construction of floors, roofs, and bridge decks is known as a reinforced concrete slab (Al-Gasham et al.,2019; Elliott,2017; Mata, 2022) A building's floor system may consist of precast components, ribbed slabs, or in-situ solid slabs. Slabs may span in one or two directions and be supported by concrete or steel beams, walls, or the structure's columns directly (Al-Azzawi and Abed, 2017; Al-Fakher et al., 2021; Alfeehan et al., 2017; Al-Gasham et al.,2021).

*Corresponding author

Peer review under the responsibility of University of Baghdad.

<https://doi.org/10.31026/j.eng.2024.10.04>



This is an open access article under the CC BY 4 license (<http://creativecommons.org/licenses/by/4.0/>).

Article received: 22/10/2023

Article revised: 21/08/2024

Article accepted: 28/09/2024

Article published: 01/10/2024



There have been several attempts to lighten concrete slabs while maintaining their flexural strength (Ammari, 2020; Al-Azzawi and Al-Asdi, 2017). This will reduce deflection and enable the use of greater spans. For flexural strength, the slab's top zone requires concrete to create a compression block, and the tension zone requires concrete to join with reinforcement (Pershakov, 2016; Vakhshouri, 2017; Plizzari and Mindess, 2019). To transmit stresses, the top and bottom slab faces also need to be connected. Long-span slab buildings can be made lighter by using beam-block slab systems, hollow core slab systems, bubble slab systems, and waffle slab systems (Abdulah, 2015; Sayhood, 2017; Haggag and Abd Elsalam, 2020; Al-Azzawi and Mtashar, 2023).

Concrete members may require strengthening and repair during the duration of their service life (Taffese and Sistonen, 2017; Alexander and Beushausen, 2019). This requirement may be necessitated by issues with the design or construction, functional modifications, design code updates, lack of maintenance, changes to the structural system, increased traffic volumes, damage accumulated over time or brought on by unpredicted overloading, fires, or earthquakes, as well as problems with blasts and explosions (Amran et al., 2018; Naser et al., 2019; Wang et al., 2021). Because it would be extremely expensive to replace deficient structures, strengthening has been chosen as the most effective way to increase their load-bearing capacity and durability (De Santis et al., 2016; Siddiqui et al., 2018). Although complete replacement of a defective or damaged part is preferable, strengthening/repair is generally more inexpensive, and civil engineering infrastructure renewal has garnered substantial attention in recent times globally (Heiza et al., 2014; Randl and Harsányi, 2018; Pöhler et al., 2021; Al-Azzawi and Mtashar, 2023). Many researchers investigate the behavior of voided slabs experimentally and theoretically by using the finite element method (Aguado et al., 2016; Li et al., 2018). ABAQUS represents the best finite element-specialized software for a wide range of purposes (Labibzadeh, 2015; Wang et al., 2017). It is commonly employed for modeling structural members. The numerical model is constructed using a combination of the input file and graphical user interface techniques (Raza and Ahmad, 2019; Lee et al., 2020; Al Hasani et al., 2021).

(Genikomsou and Polak, 2015) investigate the punching shear behavior by the nonlinear finite element of reinforced concrete slab-column connections under static and pseudo-dynamic loadings. (Vijayan, 2018) investigated Bubble-deck slabs with elliptical balls only and bubble-deck slabs with elliptical balls and GFRP strips were tested under uniformly distributed load with appropriate boundary conditions by using finite elements. (Zhou, 2018) studied the numerical investigation by the ABAQUS program of the structural behavior of basalt fiber-reinforced polymer (BFRP)-reinforced SCC deck slabs in a real bridge, named Thompson Bridge. (Al Ajami, 2018) studied punching shear behavior for flat slab specimens reinforced with glass fiber-reinforced polymer (GFRP) and steel bar materials. (Gholamhoseini, 2018) investigate experimentally and theoretically by finite element the ultimate strength of continuous composite concrete slabs with steel decking. (Elharouney, 2021) demonstrates a Finite Element (FE) analysis technique to predict the responses of the PHCSs with openings, either unstrengthened or strengthened with NSM strips.

This study divided the voided slabs into two main groups: the first group consisted of three slabs cast and tested experimentally and theoretically under monotonic loading. The second group consisted of three slabs also but tested under repeated loading experimentally and theoretically. An additional parametric study consists of fourteen slabs proposed in the ABAQUS program that is tested theoretically under monotonic and repeated loading with the following variables void shape (cylindrical and cubic voids), different reinforcement

diameter ($\emptyset 10\text{mm}$ and $\emptyset 12\text{mm}$), GFRP scheme (full and partial enhancement), different boundary conditions (simply supported and fixed edges), partial and full uniform loading and different compressive strength ($f'_c = 25\text{MPa}$).

2. EXPERIMENTAL WORK

2.1 Study Parameters

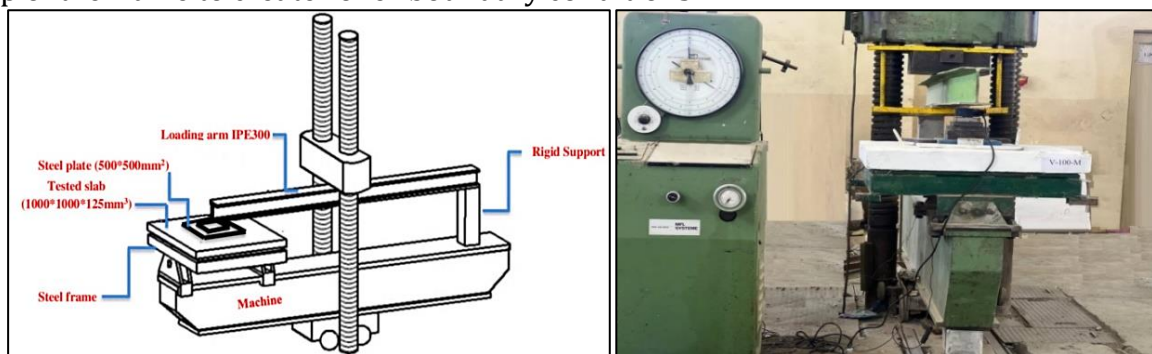
In the current work, six square two-way slabs sized $1000 \times 1000 \times 125 \text{ mm}^3$ were manufactured and tested. The form of the slab (solid or voided), the presence of GFRP sheet layers, the presence of steel fibers, and the type of loading are the primary experimental variables. **Table 1** shows details of these factors and specimen codes. Each slab code has a variety of symbols, including (S, V) referring to the solid and voided slab, (M, R) refers to the monotonic and repeated loading, (1%) denotes the presence of steel fibers in concrete, the number of GFRP layers (1GF, 2GF).

Table 1. Details of Experimental Specimens and Variables.

Slab Name	Slab Type	Steel Fibers (%)	GFRP Layers	Type of Loading
S-125-M	Solid	/	/	Monotonic
V-125-M	Voided	/	/	
V-125-1%-2GF-M	Voided	1	2	
S-125-R	Solid	/	/	Repeated
V-125-R	Voided	/	/	
V-125-1%-2GF-R	Voided	1	2	

2.2 Test Setup

At the Structural Laboratory of the Faculty of Engineering, Al-Mustansiriyah University, all slabs are tested using a hydraulically powered universal testing machine with a (3000 kN) capacity under static loads and repeated till failure. According to **Fig. 1**, the load is transmitted through a unique steel frame. The frame is made up of two components: a supporting frame and a loading arm. A steel rod with a diameter of (25) mm is welded at the top of the frame to create roller boundary conditions



(a) Test Setup.

(b) Specimen under test.

Figure 1. (a) Test Setup, (b) Specimen under test.

The loading arm is made of an IPE300 steel section, and the supporting frame is made of four C100 welded together for strong support. To ensure that the load will be distributed as a partial uniformly distributed load on the central area ($500 \times 500 \text{ mm}^2$) of the specimens, the load is transferred from the machine to the specimens by the loading arm through a set of

plates beginning with two plates of (100*100 mm²), (150*150 mm²), (300*300 mm²) and (500*500 mm²). Under the loading arm, a load cell with a 50-ton capacity has been fitted to ensure accurate loading. The deflection is measured by employing a Linear Variable Differential Transformer (LVDT) at the middle of the bottom face of each slab.

2.3 ABAQUS Modeling Process

The input software data were provided from the outcomes of laboratory investigation such as; concrete compressive strength ($f'c$), splitting tensile strength (f_t), and Modulus of elasticity (E_c). Verification would be made for three samples of the specimens cast in the laboratory listed below under both monotonic and repeated loading:

- 1- S-125-M and S-125-R
- 2-V-125-M and V-125-R
- 3-V-125-1%-2GF-M and V-125-1%-2GF-R

The items below represent the details of one model which is a solid slab called (S-125-M) which was cast and tested in the experimental work to compare the results of the finite element with the experimental results that were given in chapter four. The other models with their variables will be created and analyzed in the program and the results will be reviewed and discussed.

2.3.1 Creating Part

According to the experimental work mentioned earlier, the parts (concrete, steel reinforcement, loading plate, and support) are created with specified names in the program as shown in **Table 2**. Firstly, draw each cross-section to create the parts, and then extrude to make the parts. A 3D solid part is used for modeling the support, loading plate, and concrete also the wire part is selected for modeling the steel reinforcement. **Figs. 2 to 5** represent the parts of the model.

Table 2. Details of the parts.

No.	Part Name	Type	Shape	Feature Type
1	Concrete	3D deformable	Solid	Extrusion
2	Bar 10	3D deformable	Wire	Truss
3	Load plate	3D deformable	Solid	Extrusion
4	Support	3D deformable	Solid	Extrusion

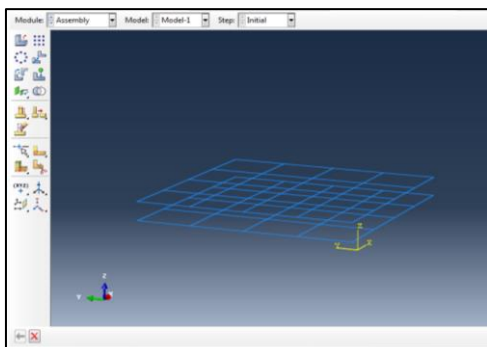


Figure 2. Steel reinforcement modeling.

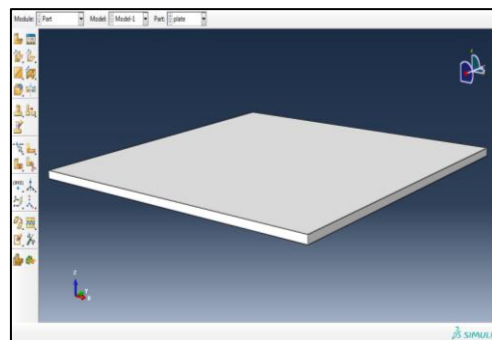


Figure 3. Loading plate modeling.

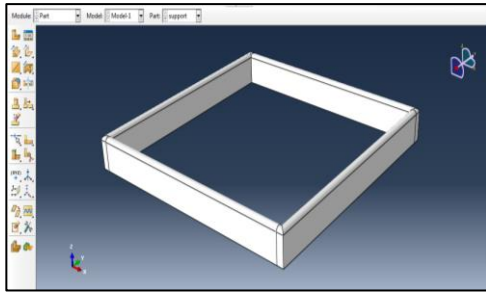


Figure 4. Support modeling.

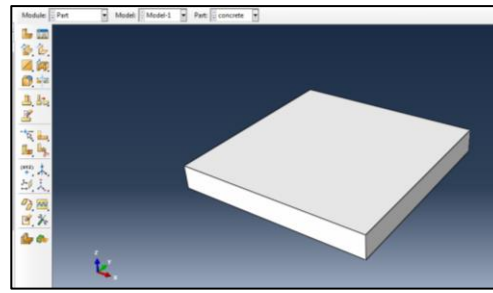


Figure 5. Concrete slab modeling.

2.3.2 Materials Properties

2.3.2.1 Concrete Property

Different model approaches exist, some of which model is based on elasticity and some on plasticity, to show how concrete slabs respond to varied stresses. Here, there are two methods for modeling and analyzing concrete materials in ABAQUS:

- 1- Standard material comprises damaged plasticity (CDP).
- 2- Standard material comprises smeared cracking (CSC).

The CDP model is preferable to use than the CSC model because it is more stable. Also, because of the best representation of the reinforced concrete mechanical behavior under different conditions of loading, the CDP model is commonly used. The required parameters by the CDP are given in **Table 3 (Ahmed, 2014; Michal and Andrzej, 2015)**.

1. Dilation angle (ψ); this parameter is applied to define the plastic flow potential. In ABAQUS the value of (ψ) ranges from (0 to 56) depending on the value of ($f'c$).
2. The flow potential eccentricity (ϵ), (0.1) is the default value.
3. The initial equi-biaxial yield stress divided by the initial uni-axial compressive yield stress ($Fb0/Fc0$) equals 1.16.
4. (Kc) is defined as; the parameter which is used for determining the yield surface of the concrete plasticity model. The value of (Kc) is ranged from (0.5 to 1), in this study the used default value is (0.667).
5. A viscosity parameter; that is defined as visco-plastic regularization (μ), the default value in ABAQUS is (0). The concrete properties are shown in **Table 3 (Hibbitt et al., 2016; Barbero, 2023)**.

Table 3. Concrete Properties.

	Property	Value
Elastic properties	Density (assumed)	2.4 g/cm ³
	Modulus of Elasticity ($4700\sqrt{f'_c}$)	30784 MPa
	Poisson's ratio	0.2
	Plastic properties CDP	
Plasticity	Dilation Angle	38
	Eccentricity	0.1
	Fb0/Fc0	1.16
	K	0.667
	Viscosity Parameter	0.001-0.00001
Compressive behavior	From compressive strength test	
Tensile behavior	From splitting tensile strength test	

2.3.2.2 Steel Reinforcement Property

In this analysis, the steel reinforcement stress-strain curve is taken from the experimental tensile test and simplified to elastic-perfectly plastic behavior. The numerical properties that are needed for the inputs of the program as shown in **Table 4**.

Table 4. Steel reinforcement properties.

	Property	Value
Elastic properties	Density (assumed)	78.5kN/m ³
	Modulus of Elasticity (assumed)	200,000 MPa
	Poisson's ratio	0.3
Plastic	Yield Stress and Plastic Strain (from the tensile test of reinforcement)	$f_y = 553$ MPa $f_u = 644.3$ MPa

2.3.2.3 Loading Plate and Support Properties

The properties of the loading plate and support depend on mechanical properties inputs in the program which is linear elastic as shown in **Table 5**.

Table 5. Loading plate and support properties.

	Property	Value
Elastic	Modulus of Elasticity	200,000 MPa
	Poisson's ratio	0.3

2.3.3 Interaction

This feature is used to connect many components so that they act as one unit (**Yuan et al., 2021**). After assembly of all the parts/model instances, the longitudinal and the transverse reinforcement steel bars are embedded in the concrete by using embedded region constraints. On the other side, the lower face of the concrete member is tied to the face of the supports while the upper concrete face is tied to the loading plate as shown in **Fig. 6**.

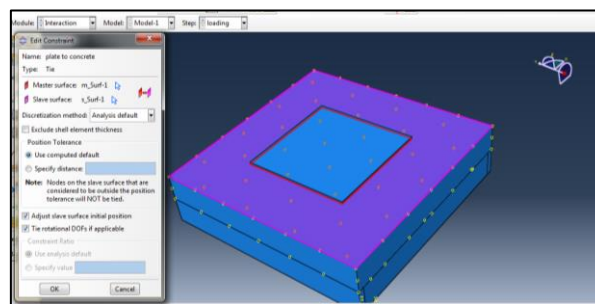


Figure 6. Interaction between the concrete and loading plate.

2.3.4 Meshing

For structured models, 3D 8-node hexahedral brick element components with reduced integration (C3D8) are used. For the transverse reinforcement component of this item, truss T3D2 (A2-linear knot3-d) (**Manual, 2014**) The element size of 20mm cubic was chosen for this investigation to balance time consumption and result accuracy. **Fig. 7** illustrates the ABAQUS mesh model for the modeled specimen.

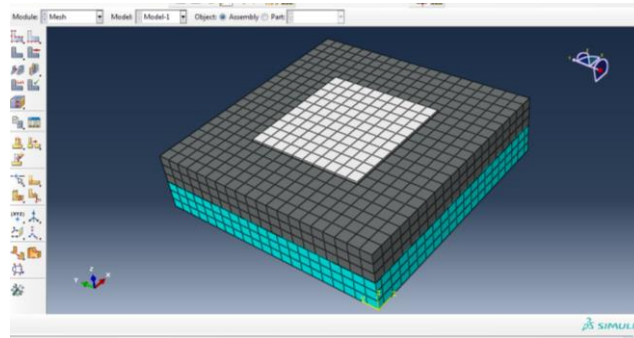


Figure 7. Model mesh.

2.3.5 Load And Support Boundary Conditions

Larger values than the ultimate loads for tested specimens are entered into ABAQUS as an applied load in the form of a partially applied load (Wu et al., 2014). The software will apply the load in steps of increment until it reaches the final increment with the ultimate load. Boundary conditions are applied as (displacement) with constrain for the vertical displacement as shown in Fig. 8.

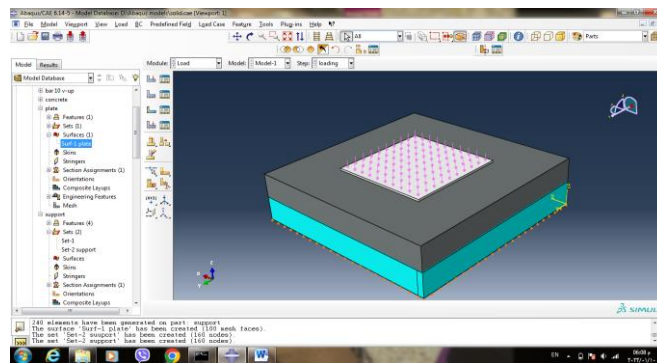


Figure 8. Loading and boundary conditions of the support.

2.4 Numerical Analysis Results

The measured values of ultimate load and displacement at the center obtained from the experimental test are compared with the finite element simulation results for the three selected concrete slabs under monotonic and repeated loading conditions. The theoretical results demonstrate a good agreement with the experimental one. The variations between the experimental and finite element results in terms of ultimate loads and ultimate deflection for all specimens are so close. The adopted models give good values with good accuracy with (10%) variation under monotonic loading as shown in Table 6.

Table 6. Experimental and theoretical results for slab specimens under monotonic loading.

Slab Specimens	Exp. Results		Theo. Results		Pu Exp./ Pu Theo.	Δu Exp./ Δu Theo.
	Pu	Δu	Pu	Δu		
S-125-M	210	6.3	220	6	0.95	1.05
V-125-M	160	9.1	172.6	8.1	0.92	1.1
V-125-1%-2GF-M	192	4.6	210.3	4	0.91	1.1

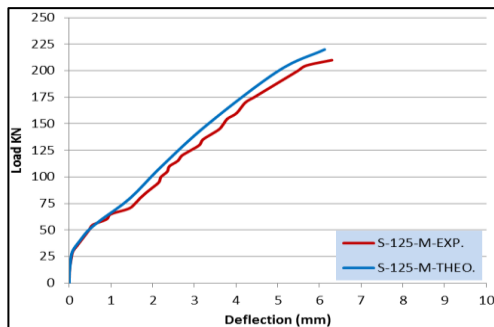


For repeated loading, the variations between the theoretical and experimental outcomes in terms of ultimate loads and ultimate deflection for all specimens are very close. The adopted models give good values with good accuracy with (10%) variation for repeated loading as shown in **Table 7**.

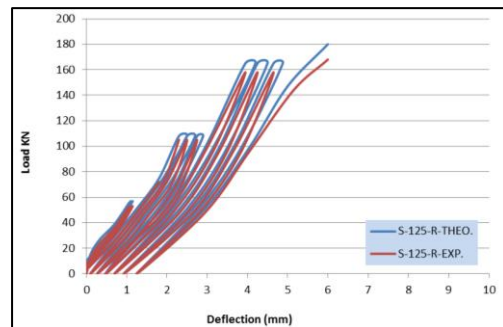
Table 7. Experimental and theoretical results for slab specimens under repeated loading.

Slab Specimens	Exp. Results		Theo. Results		Pu Exp./ Pu Theo.	Δu Exp./ Δu Theo.
	Pu	Δu	Pu	Δu		
S-125-R	168	6	180	5.8	0.93	1.03
V-125-R	125	7.8	135	7.1	0.93	1.09
V-125-1%-2GF-R	150	4.2	168	4	0.9	1.05

Figs. 9 to 11 show a comparison between the theoretical and experimental load-deflection curves for the chosen three specimens under monotonic loading and the other three specimens under repeated loading. The load-deflection curves obtained from the numerical simulation showed almost stiffer behavior in comparison with the experimental one. This is because, in finite elements, some material parameters are assumed and not measured in the laboratory and due to the adopted material model approximation.



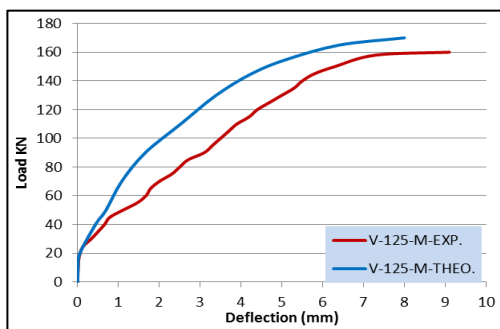
(a) Monotonic loading.



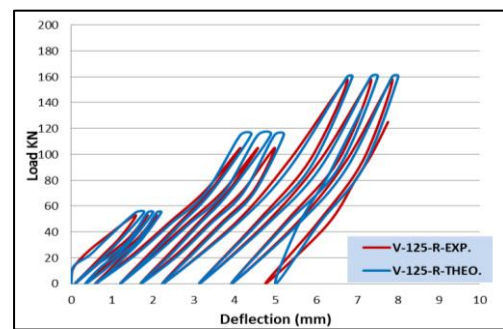
(b) Repeated loading.

Figure 9. (a) Experimental and theoretical load-deflection curve for (S-125) under monotonic loading (b) Experimental and theoretical load-deflection curve for (S-125) under repeated loading.

The largest variation in the deflection curves is obtained in the specimen (V-125-M) through the loading process while at the end of loading the variation became (10%). The rest specimens show very little variation in the ultimate load and deflection.

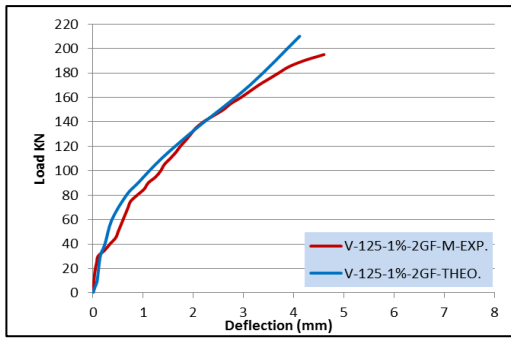


(a) Monotonic loading.

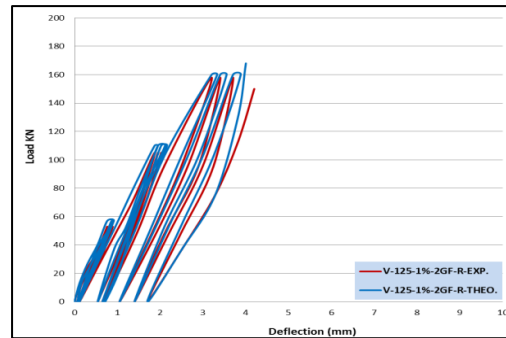


(b) Repeated loading.

Figure 10. (a) Experimental and theoretical load-deflection curve for (V-125) under monotonic loading (b) Experimental and theoretical load-deflection curve for (V-125) under repeated loading.



(a) Monotonic loading.



(b) Repeated loading.

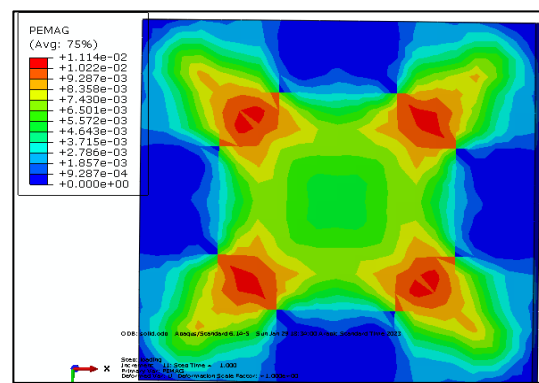
Figure 11. (a) Experimental and theoretical load-deflection curve for (V-125-1%-2GF) under monotonic loading (b) Experimental and theoretical load-deflection curve for (V-125-1%-2GF) under repeated loading.

2.5 Crack Patterns

Figs. 12-17 show a comparison of the concrete crack patterns obtained from the theoretical outcomes of the program and those found in the experimental test under monotonic and repeated loading. When the slab fails, the cracking pattern on the stress side of the slab spreads within the concrete adjacent to the center.



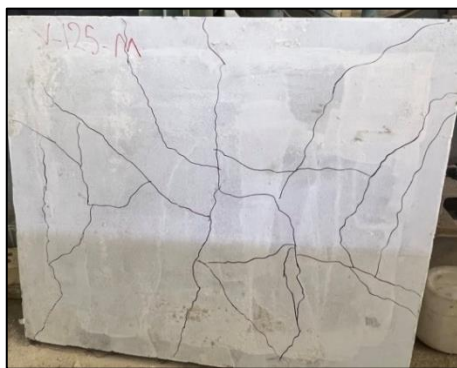
(a) Experimental model.



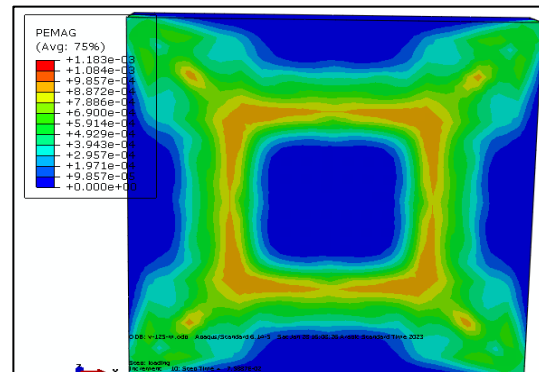
(b) Numerical model.

Figure 12. Cracking pattern for slab (S-125-M) under monotonic load.

With increasing load, the cracks propagate tangentially near the center and then spread radially. When the maximum principal plastic strain is positive, the concrete weakened or damaged plasticity model assumes that cracking begins.



(a) Experimental model.



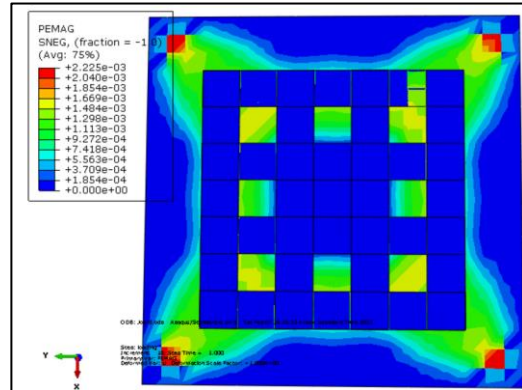
(b) Numerical model.

Figure 13. Cracking pattern for slab (V-125-M) under monotonic load.

The cracks are thought to be perpendicular to the maximum principal plastic strains, allowing the cracking direction to be seen through the maximum principal plastic strains. The blue color contour in the figures shows that the concrete has a lower strain, while the other color shows the development of micro-cracks before the concrete begins to yield. Comparable outcomes in terms of stress contours are obtained.

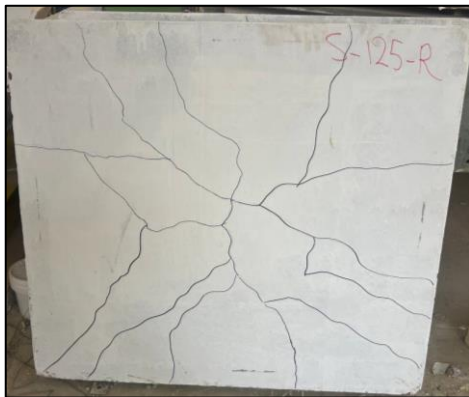


(a) Experimental model.

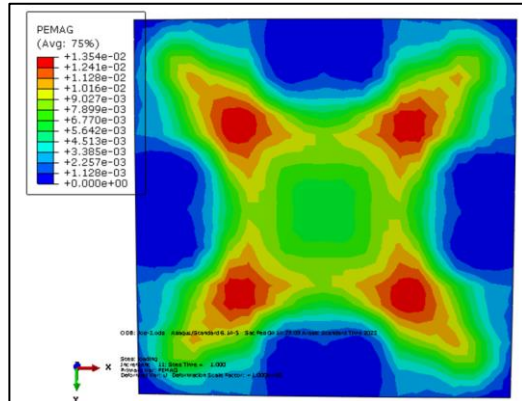


(b) Numerical model.

Figure 14. Cracking pattern for slab (V-125-15-2GF-M) under monotonic load.



(a) Experimental model.

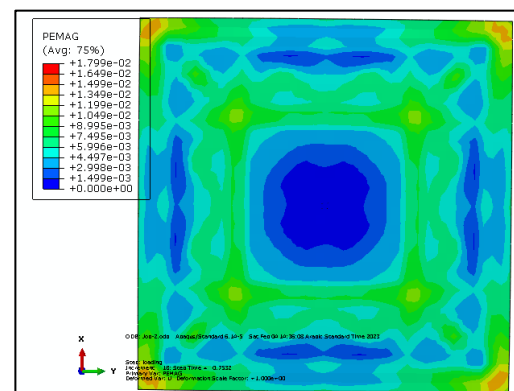


(b) Numerical model.

Figure 15. Cracking pattern for slab (S-125-R) under repeated load.

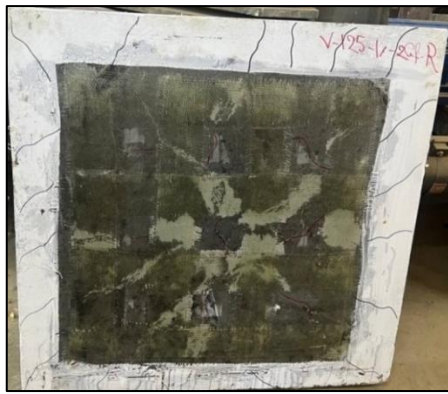


(a) Experimental model.

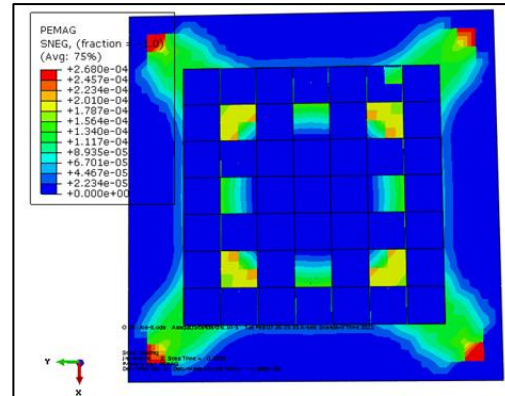


(b) Numerical model.

Figure 16. Cracking pattern for slab (V-125-R) under repeated load.



(a) Experimental model.



(b) Numerical model.

Figure 17. Cracking pattern for slab (V-125-1%-2GF-R) under repeated load.

2.6 Parametric Study

In this part, new variables have been investigated that affect the behavior of reinforced concrete slabs and are not implemented in the experimental part of this study. These specimens are divided into two groups according to the nature of loading.

2.6.1 Slabs Under Monotonic Loading

Seven slabs proposed by the same procedure and the same properties in the ABAQUS program are tested theoretically under monotonic loading with the following variables:

- 1- Void shape (cylindrical and cubic voids).
- 2- Different reinforcement diameter ($\varnothing 10\text{mm}$ and $\varnothing 12\text{mm}$).
- 3- GFRP scheme (full and partial enhancement).
- 4- Different boundary conditions (simply supported and fixed edges).
- 5- Partial and full uniform loading.
- 6- Different compressive strength ($f'_c = 25\text{MPa}$)

2.6.1.1 Load-Deflection Relationship

Ultimate loads and a final deflection taken at the center of the bottom face of the slabs are observed and recorded by FEA as well as; the energy absorption under the curves of deflection is computed by the trapezoidal rule as shown in **Table 8**.

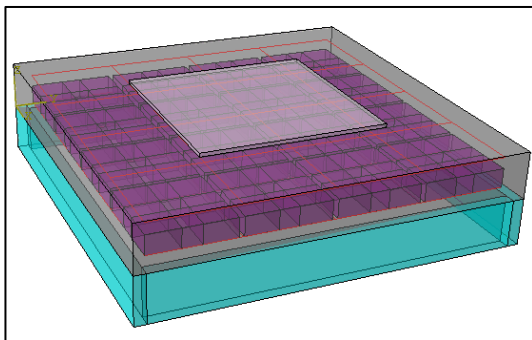
Table 8. Theoretical results for slab specimens under monotonic loading.

Slab Specimens	Variables	Pu	Δu	Energy Absorption (KN.mm)
V-125-M	Cylindrical voids	175	7.6	850.6
V-125-M	($\varnothing 12\text{mm}$) Bar	190	6.9	900.56
V-125-1%-2GF-M	Full GFRP	195	5.5	1310.66
S-125-M	Fixed edges	241	5.5	937.2
V-125-M	Full uniform loading	145	8.5	628.25
V-125-M	$f'_c = 25\text{MPa}$	93	5.3	513.44
V-125-2GF-M		107	4.2	718.8

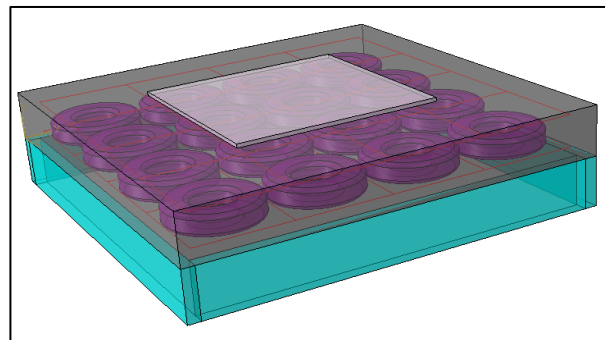
In general, using cylindrical voids instead of cubic ones with a similar volume of the void as shown in **Fig. 18** doesn't affect both ultimate load and final deflection (3% variation); while the energy absorption increased by (17%) as shown in **Fig. 19**. The ultimate load increases when using reinforcing bars of (\varnothing 12mm) compared to (\varnothing 10mm) by (11%) while the deflection decreased by (23%) and the energy absorption increased by (21.6%) due to the increase in the moment capacity of the section as shown in **Fig. 20**.

Strengthening the slab with two layers of GFRP sheets of ($700 \times 700 \text{ mm}^2$) in the bottom face comparable to the slab enhanced by four strips (two layers) of GFRP on both sides ($100 \times 700 \text{ mm}^2$) shows a remarkable increase in deflection by (25%) and a decrease in ultimate load and energy absorption by (7% and 3%) respectively as shown in **Fig. 21**, so the scheme of GFRP sheets (less width and more strips) is more effective in decreasing the deflection.

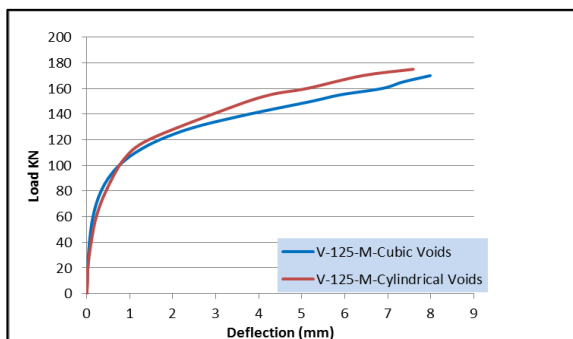
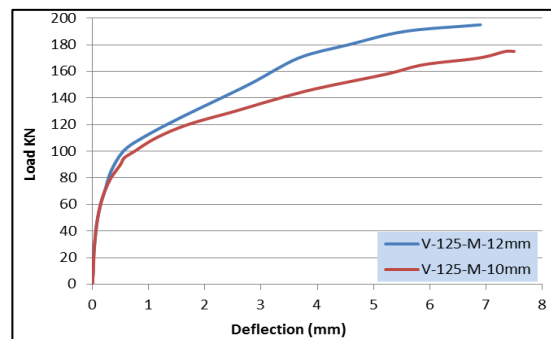
Supporting the solid slab on fixed edges instead of simply supporting one led to an increase in the ultimate load and energy absorption by (15% and 12%) respectively while the deflection decreased by (14.5%) due to the high moment capacity of the section as shown in **Fig. 22**. When the voided slab is fully loaded on the top face; the ultimate load and energy absorption decrease by (15% and 11%) respectively and the deflection increases by (6%) due to the distribution of the loads on a large area than the area of partial uniform loading as shown in **Fig. 23**. Using compressive strength equal to (25MPa) without steel fibers in voided slab strengthened by two layers of GFRP sheets lead to an increase in the ultimate load by (15%) and a decrease in the deflection by (26%) while the energy absorption increased by (40%) compared to unstrengthened slab with same properties as shown in **Fig. 24**. This can be attributed to the presence of GFRP sheets which prevent cracks propagation and increase the stiffness and rigidity of slabs.



(a) Cubic voids.



(b) Cylindrical voids.

Figure 18. Cubic and cylindrical voids in voided slab.**Figure 19.** Load-deflection relationship for slabs with (cubic and circular voids).**Figure 20.** Load-deflection relationship for voided slabs of (\varnothing 10 and 12 mm).

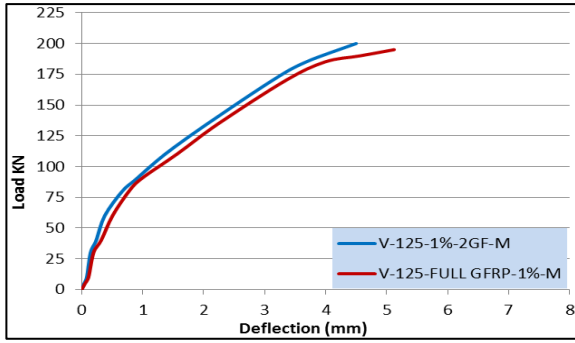


Figure 21. Load-deflection relationship for slabs with (full and partial GFRP).

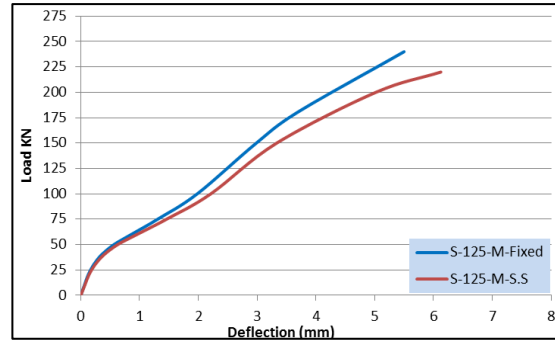


Figure 22. Load-deflection relationship for slabs with different B.C.

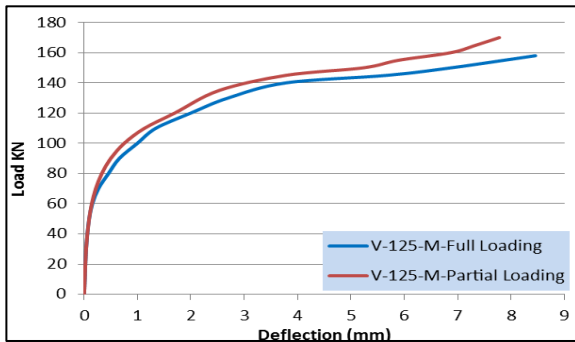


Figure 23. Load-deflection relationship for slabs with partial and full loading.

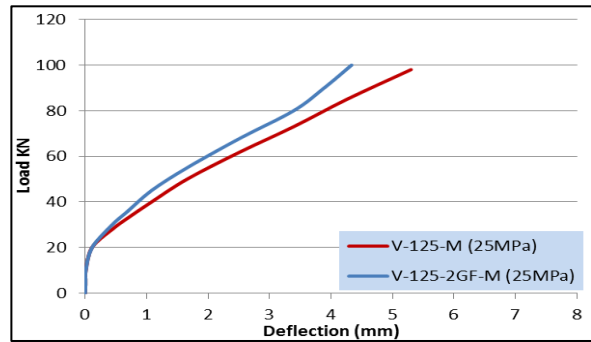


Figure 24. Load-deflection relationship for slabs with ($f'c=25\text{MPa}$).

2.6.1.2 Crack Patterns

Figs. 25-31 show the crack patterns of the modeled specimens under monotonic loading with different variables (cylindrical voids, $\varnothing 12\text{mm}$ bar diameter, full strengthening by GFRP, fixed edges, fully loaded slab, and $f'c=25\text{MPa}$). The blue contours plot of the slabs indicates concrete elastic behavior whereas the other color indicates the formation of micro-cracks until the beginning of the concrete yielding. The orange color refers to the places of crack and the red color indicates full concrete failure.

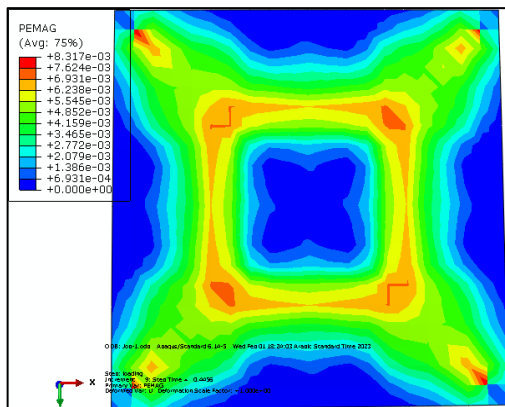


Figure 25. Crack pattern for a modeled slab with cylindrical voids.

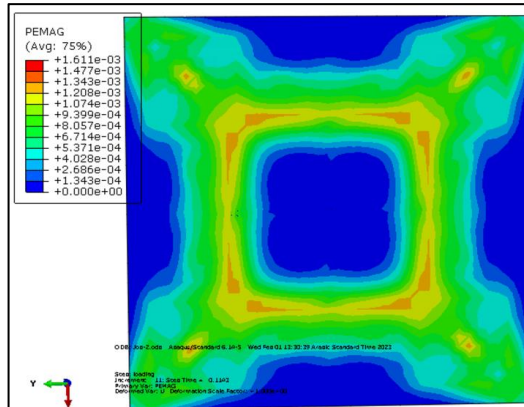


Figure 26. Crack pattern for a modeled voided slab with $\varnothing 12\text{ mm}$.

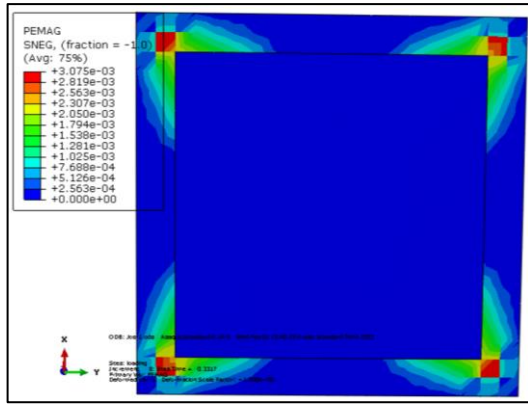


Figure 27. Crack pattern for a modeled voided slab with full GFRP.

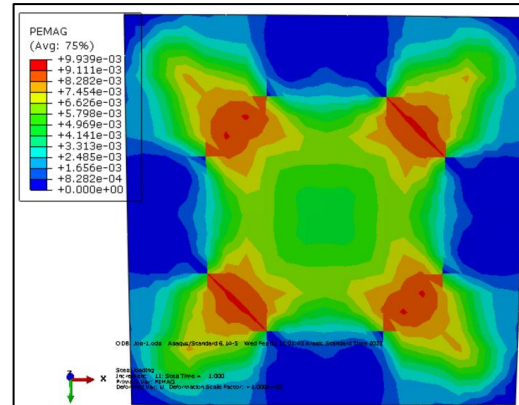


Figure 28. Crack pattern for a modeled solid slab with fixed edges.

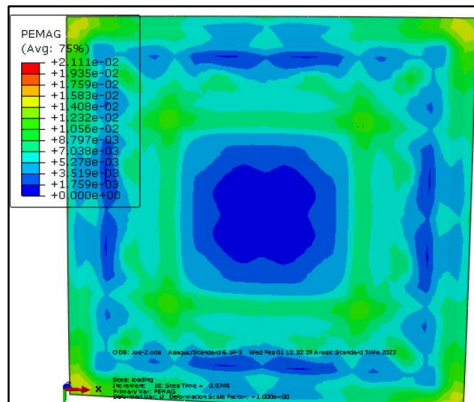


Figure 29. Crack pattern for a modeled fully loaded voided slab.

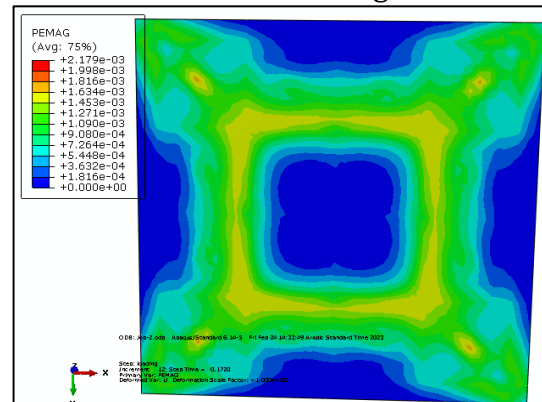


Figure 30. Crack pattern for a modeled voided slab ($f'c=25\text{MPa}$).

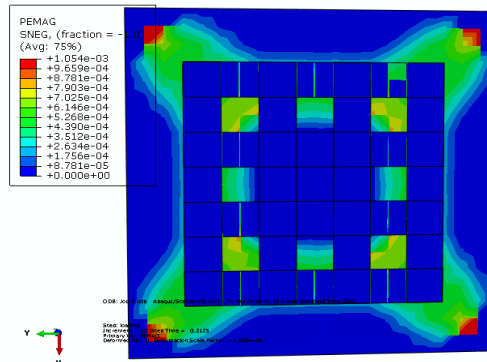


Figure 31. Crack pattern and vertical displacement for a voided slab ($f'c=25\text{MPa}$ with GFRP).

The crack pattern had approximately the same patterns for all the modeled slabs except the fully loading specimens where the shape of cracks are completely different due to distributing the loads over the whole top surface uniformly, as shown in Fig. 29.

2.6.2 Slabs Under Repeated Loading

Seven slabs were made by the same procedure and the same properties in the ABAQUS program and tested under repeated loading with the same variables mentioned in (2.6.1).

2.6.2.1 Load-Deflection Relationship

Ultimate loads and a final deflection taken at the center of the bottom face of the slabs are observed and recorded by FEA as well as; the energy absorption under the curves of deflection is computed in the same manner as shown in **Table 9**.

Table 9. Theoretical results for slab specimens under repeated loading.

Slab Specimens	Variables	Pu	Δu	Energy Absorption (KN.mm)
V-125-R	Cylindrical voids	160	7.2	672
V-125-R	($\emptyset 12\text{mm}$) Bar	170	6.2	730
V-125-1%-2GF-R	Full GFRP	178	5.1	1048.5
S-125-R	Fixed edges	195	5.5	930
V-125-R	Full uniform loading	125	7.6	500.5
V-125-M	$f'c = 25 \text{ MPa}$	80	5.5	436.4
V-125-2GF-M		98	5	589.5

In general, using cylindrical voids instead of cubic ones under repeated loading lead to an increase in the ultimate load and energy absorption by (15.6% and 12%) while the deflection remains the same compared to the slab with cubic voids as shown in **Fig. 32**. The ultimate load and energy absorption increases when using reinforcing bars of ($\emptyset 12\text{mm}$) compared to ($\emptyset 10\text{mm}$) by (20.5% and 18%) while the deflection decreased by (14.5%) under repeated loading due to increasing the stiffness of the slab as shown in **Fig. 33**. Strengthening the slab with a double sheet of GFRP ($700 \times 700 \text{ mm}^2$) in the bottom face comparable to the slab enhanced by four double strips of GFRP on both sides ($100 \times 700 \text{ mm}^2$) shows an increase in ultimate load and deflection by (21.5% and 15.7%) respectively while the energy absorption decreased by (5%) under repeated loads as shown in **Fig. 34**.

Supporting the solid slab on fixed edges instead of simply supporting one under repeated loading led to an increase in the ultimate load and energy absorption by (8% and 19%) respectively while the deflection decreased by (5%) as shown in **Fig. 35**. When the voided slab is fully loaded on the top face and loaded repeatedly; the ultimate load and energy absorption decreased by (8% and 20%) while the deflection increased by (7%) compared to the partial uniform loading as shown in **Fig. 36**.

Using compressive strength equal to (25MPa) without steel fibers in voided slab strengthened by two layers of GFRP sheets lead to an increase in the ultimate load by (18.4%) and a decrease in the deflection by (10%) while the energy absorption increased by (30%) compared to unstrengthen slab with same properties as shown in **Fig. 37**.

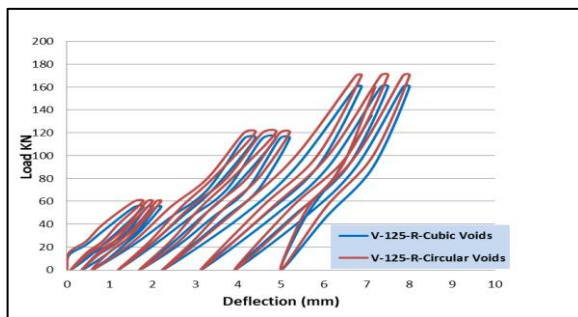


Figure 32 Load-deflection relationship for slabs with (cubic and cylindrical voids).

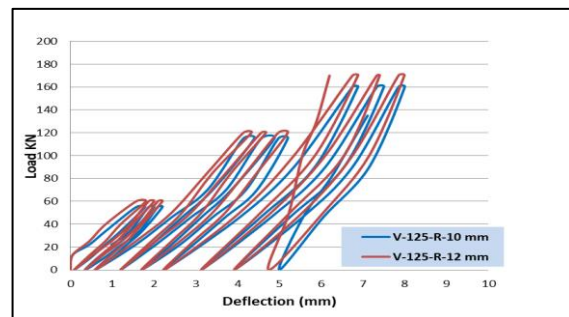


Figure 33 Load-deflection relationship for voided slabs of ($\emptyset 10$ and 12 mm).

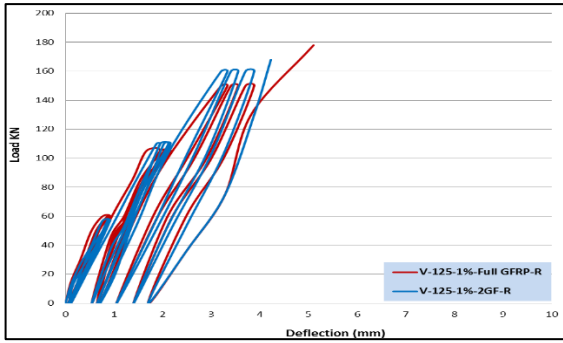


Figure. 34 Load-deflection relationship for slabs with (full and partial GFRP).

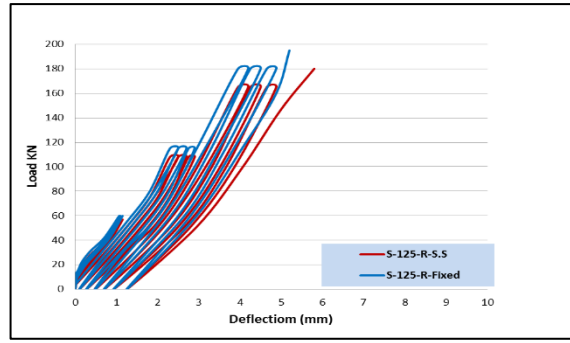


Figure. 35 Load-deflection relationship for slabs with different B.C.

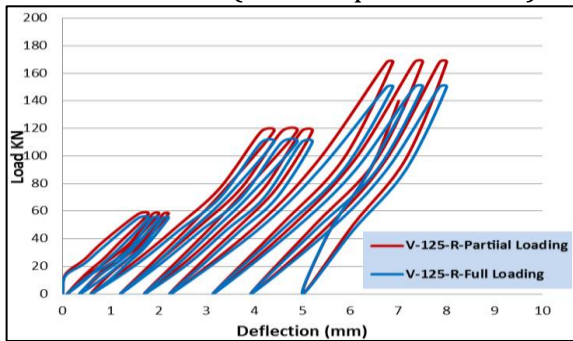


Figure. 36 Load-deflection relationship for slabs with partial and full loading.

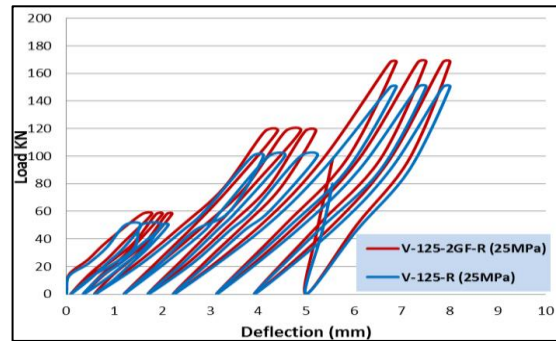


Figure. 37 Load-deflection relationship for slabs with ($f'c=25MPa$).

This can be attributed to the presence of GFRP sheets which prevent cracks propagation and increase the stiffness and rigidity of slabs. In general; it can be concluded that the ultimate load and energy absorption for models tested under repeated loads is decreased by approximately (15-20%) compared to models tested under monotonic loading due to loading and unloading cycles.

2.6.2.2 Crack Patterns

It was noticed that the crack pattern of the slab specimens that were subjected to repeated loading processes were nearly similar to that of the specimens under static load. In addition, there are further vertical cracks in the bottom face due to loading and unloading cycles and resisting more loads as shown in Figs. 38 - 44.

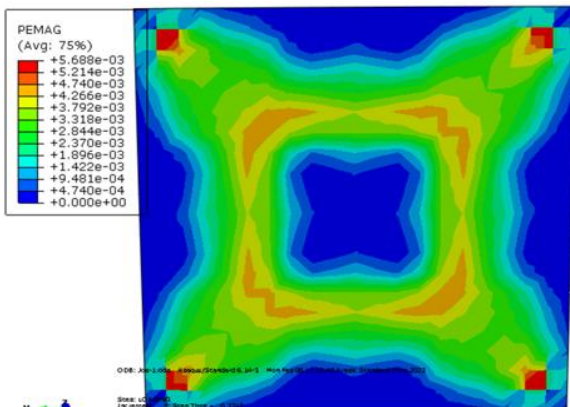


Figure. 38 Crack pattern for a modeled slab with cylindrical voids.

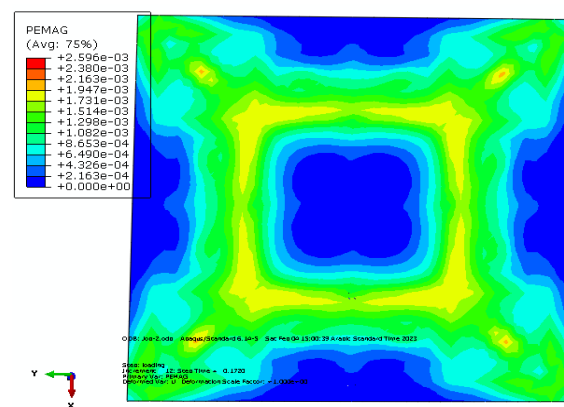


Figure. 39 Crack pattern for a modeled voided slab with $\varnothing 12$ mm.

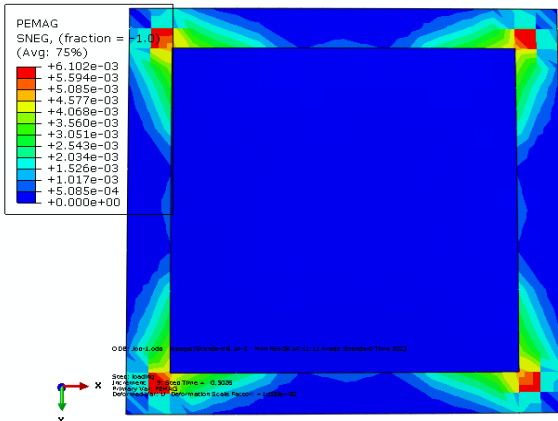


Figure. 40 Crack pattern for a modeled voided slab with full GFRP.

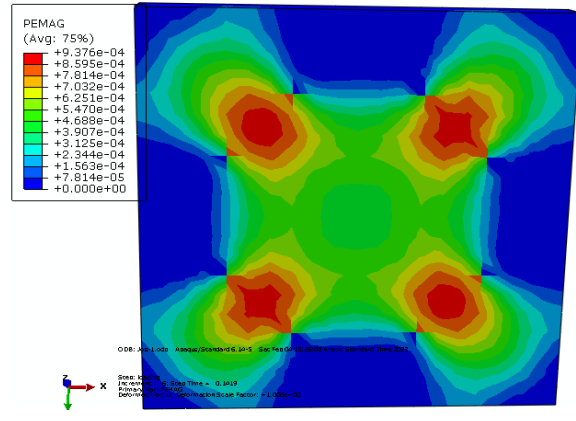


Figure. 41 Crack pattern for a modeled voided slab of fixed edges.

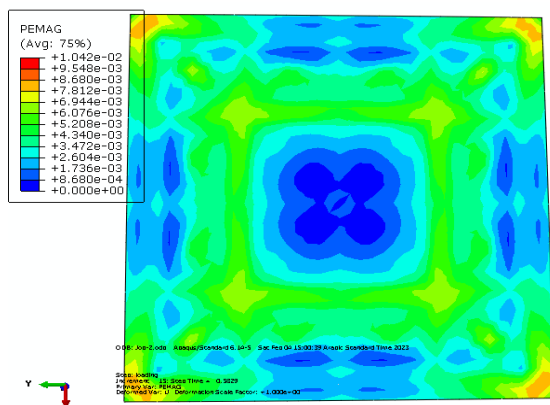


Figure. 42 Crack pattern for a modeled fully loaded voided slab.

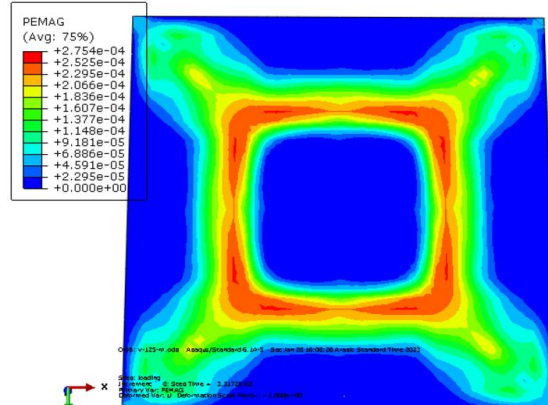


Figure. 43 Crack pattern for a modeled voided slab ($f'c=25\text{MPa}$).

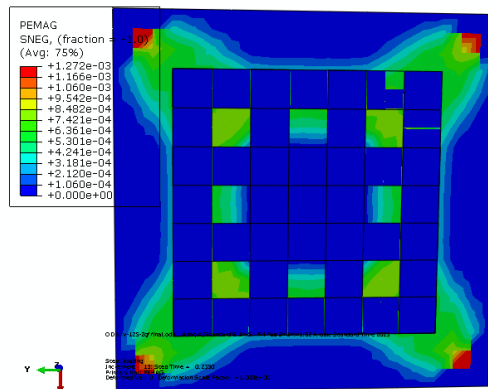


Figure. 44 Crack pattern and vertical displacement for a voided slab ($f'c=25\text{MPa}$ with GFRP).

3. CONCLUSIONS

1. In general, it can be concluded that the ultimate load and energy absorption for models tested under repeated loads is decreased by approximately (15-20%) compared to models tested under monotonic loading due to loading and unloading cycles.
2. The finite element models that were used in this study can be used successfully for the modeling of the two-way voided slabs as it agrees well with the experimental results which makes a parametric study reliable and acceptable. The created finite element



- models can accurately reflect the test results with an acceptable degree of difference in deflection and ultimate load by 10%.
3. The crack patterns obtained for the analyzed specimens using finite element models under monotonic and repeated loading are nearly identical to the crack patterns observed in the experimental work.
 4. Replacing the cubic voids in the voided slabs by cylindrical one of the same volume in the ABAQUS program showed very little effect not exceeding (3%) in both ultimate load and final deflection while the energy absorption increased by (17%).
 5. Using ($\varnothing 12$ mm) bar as reinforcement instead of ($\varnothing 10$ mm) resulted in a decrease in the final deflection by (23%) and the energy absorption increased by (21.6%).
 6. Strengthening the bottom face of the voided slab with four strips of GFRP sheets in both directions is more effective in decreasing the deflection by (25%) than full strengthening by GFRP sheet.
 7. Supporting the solid slab on fixed edges instead of simply supporting one led to an increase in the ultimate load and energy absorption by (15% and 12%) respectively while the deflection decreased by (14.5%).
 8. Using compressive strength equal to (25MPa) without steel fibers in a voided slab strengthened by two layers of GFRP sheets lead to a further increase in the ultimate load and energy absorption by (15% and 40%) respectively and a decrease in the deflection by (26%) compared to unstrengthen slab with same properties.

NOMENCLATURE

Symbol	Description
S-t-SS-L-M	Solid or Voided Slab-Slab thickness - Steel fiber percentage - Treatment layer of GFRP- Type of applied load Repeated or Monotonic
S-125-M	Solid slab- 125mm thickness - monotonic load
V-125-M	voided slab- 125mm thickness -monotonic load
V-125-1%-2GF-M	voided slab-125mm thickness-1% steel fiber - two layer -monotonic load
S-125-R	Solid slab- 125mm thickness - repeated load
V-125-R	voided slab- 125mm thickness - repeated load
V-125-1%-2GF-R	voided slab-125mm thickness-1% steel fiber - two layer -repeated load

Acknowledgements

The authors express their sincere thanks to the Civil Engineering Department, University of AL- NAHRAIN for their encouragement and support.

Credit Authorship Contribution Statement

Shahad H. Mtashar: Writing –review & editing, Writing –original draft, Validation, Software, Methodology. Adel A. Al-Azzawi: editing and supervised the manuscript.

Declaration of Competing Interest

The authors declare that they have no known competing financial interests or personal relationships that could have appeared to influence the work reported in this paper.



REFERENCES

- Abdullah, M., 2015. Behavior of reinforced lightweight concrete two way slabs strengthened with CFRP sheets. *Engineering and Technology Journal*, 33(8A), pp. 1813–1829.
- Aguado, J.V., Albero, V., Espinos, A., Hospitaler, A. and Romero, M.L., 2016. A 3D finite element model for predicting the fire behavior of hollow-core slabs. *Engineering Structures*, 108, pp. 12–27. <https://doi.org/10.1016/j.engstruct.2015.11.008>.
- Ahmed, A., 2014. Modeling of a reinforced concrete beam subjected to impact vibration using ABAQUS. *International Journal of Civil and Structural Engineering*, 4(3). <https://doi.org/10.6088/ijcser.201304010023>.
- Ajami, A. Al, 2018. Punching shear of concrete flat slabs reinforced with fiber reinforced polymer bars, PhD Thesis, University of Bradford, England. <http://hdl.handle.net/10454/16864>
- Al Hasani, S., Nasrellah, H. A. and Abdulraeg, A.A., 2021. Numerical study of reinforced concrete beam by using ABAQUS software. *International Journal of Innovative Technology and Interdisciplinary Sciences*, 4(3), pp. 733–741. <https://doi.org/10.15157/ijitis.2021.4.3.733-741>.
- Al-Azzawi, A. and Mtashar, S., 2023a. Response of two-way reinforced concrete voided slabs enhanced by steel fibers and GFRP sheets under monotonic loading. *Structural Monitoring and Maintenance*, 10(1), pp. 1–23. <https://doi.org/10.12989/smm.2023.10.1.001>.
- Al-Azzawi, A.A. and Abed, S.A., 2017. Investigation of the behavior of reinforced concrete hollow-core thick slabs. *Computers and Concrete*, 19(5), pp. 567–577. <https://doi.org/10.12989/cac.2017.19.5.567>.
- Al-Azzawi, A.A. and Mtashar, S.H., 2023b. Behavior of two-way reinforced concrete voided slabs enhanced by steel fibers and GFRP sheets under repeated loading. *Results in Engineering*, 17, P. 100872. <https://doi.org/10.1016/j.rineng.2022.100872>.
- Al-Azzawi, A.A., Abbas J and Al-Asdi, 2017. Behavior of one way reinforced concrete slabs with styropor blocks. *Advances in Concrete Construction*, 5(5), P. 451. <https://doi.org/10.12989/acc.2017.5.5.451>.
- Amran, Y.M., Alyousef, R., Rashid, R.S., Alabduljabbar, H. and Hung, C.C., 2018, November. Properties and applications of FRP in strengthening RC structures: A review. In *Structures* (Vol. 16, pp. 208-238). Elsevier. <https://doi.org/10.1016/j.istruc.2018.09.008>.
- Alexander, M. and Beushausen, H., 2019. Durability, service life prediction, and modelling for reinforced concrete structures – review and critique. *Cement and Concrete Research*, 122, pp. 17–29. <https://doi.org/10.1016/j.cemconres.2019.04.018>.
- Al-Fakher, U., Manalo, A., Ferdous, W., Aravinthan, T., Zhuge, Y., Bai, Y. and Edo, A., 2021. Bending behaviour of precast concrete slab with externally flanged hollow FRP tubes. *Engineering Structures*, 241(112433), P. 112433. <https://doi.org/10.1016/j.engstruct.2021.112433>.
- Al-Gasham, T.S., Hilo, A.N. and Alawsi, M.A., 2019. Structural behavior of reinforced concrete one-way slabs voided by polystyrene balls. *Case Studies in Construction Materials*, 11, P. 00292. <https://doi.org/10.1016/j.cscm.2019.e00292>.
- Al-Gasham, T.S., Mhalhal, J.M. and Abid, S.R., 2021. Quasi-static analysis of biaxial voided slabs with openings. *Structures*, 33(4176-4192), pp. 4176–4192. <https://doi.org/10.1016/j.istruc.2021.07.021>.
- Ammari, M.S., Belhadj, B., Bederina, M., Ferhat, A. and Quéneudec, M., 2020. Contribution of hybrid



fibers on the improvement of sand concrete properties: Barley straws treated with hot water and steel fibers. *Construction and Building Materials*, 233, P. 117374. <https://doi.org/10.1016/j.conbuildmat.2019.117374>.

Ashraf Abdulhadi Alfeehan, Hassan Issa Abdulkareem and Shahad Hameed Mutashar, 2017. Flexural behavior of sustainable reactive powder concrete bubbled slab flooring elements. *Challenge Journal of Structural Mechanics*, 3(2), pp. 81–81. <https://doi.org/10.20528/cjsmec.2017.04.010>.

Barbero, E.J., 2013. *Finite element analysis of composite materials using Abaqus*. Boca Raton, FL: Crc Press, Taylor & Francis Group.

De Santis, S., de Felice, G., Napoli, A. and Realfonzo, R., 2016. Strengthening of structures with steel reinforced polymers: A state-of-the-art review. *Composites Part B: Engineering*, 104, pp. 87–110. <https://doi.org/10.1016/j.compositesb.2016.08.025>.

Elharouney, O., Elkateb, M. and Khalil, A., 2021. Behaviour of prestressed hollow core slabs strengthened with NSM CFRP strips around openings: A finite element investigation. *Engineering Structures*, 238, P. 112262. <https://doi.org/10.1016/j.engstruct.2021.112262>.

Elliott, K.S., 2017. Historical and chronological development of precast concrete structures. *Modernisation, Mechanisation and Industrialisation of Concrete Structures*, pp. 1-60. <https://doi.org/10.1002/9781118876503.ch1>.

Genikomsou, A.S. and Polak, M.A., 2015. Finite element analysis of punching shear of concrete slabs using damaged plasticity model in ABAQUS. *Engineering Structures*, 98, pp. 38–48. <https://doi.org/10.1016/j.engstruct.2015.04.016>.

Gholamhoseini, A., 2018. Experimental and finite element study of ultimate strength of continuous composite concrete slabs with steel decking. *International Journal of Advanced Structural Engineering*, 10(1), pp. 85–97. <https://doi.org/10.1007/s40091-018-0183-3>.

Haggag, H.A., M., M. and Elsalam, A., 2020. Flexural behavior of two-way solid slabs reinforced with GFRP bars. *International Journal of Civil Engineering and Technology (IJCIET)*, 11(1), pp. 288-303. <https://doi.org/10.34218/ijciet.11.1.2020.030>.

Heiza, H., Tayel, M., Meleka, N. and Nabil, A., 2014. State-of-the art review: Strengthening of reinforced concrete structures - different strengthening techniques. *In Sixth International Conference on Nano-Technology in Construction* (Vol. 6, No. 6-C, pp. 22-24).

Hibbitt, K., Karlsson, B.I. and Sorenson, E.P., 2016. ABAQUS/Standard theory manual. *Sorenson Inc*, 421, p. 422.

Hu, H., Dong, C.Z., Wang, J. and Chen, J., 2021. Experimental study of the fatigue performance of the bonding surfaces and load-bearing capacity of a large-scale severely damaged hollow slab strengthened by CFRP. *Sustainability*, 13(21), P. 12179. <https://doi.org/10.3390/su132112179>.

Jamal, J. and Vijayan, V., 2018. A study on strengthening of bubble deck slab with elliptical balls by using GFRP sheets. *SSRN Electronic Journal*. <https://doi.org/10.2139/ssrn.3591289>.

Labibzadeh, M., 2015. The numerical simulations of the strengthened RC slabs with CFRPs using standard CDP material model of Abaqus code. *European Journal of Environmental and Civil Engineering*, 19(10), pp. 1268–1287. <https://doi.org/10.1080/19648189.2015.1013637>.

Lee, S.H., Abolmaali, A., Shin, K.J. and Lee, H.D., 2020. ABAQUS modeling for post-tensioned reinforced concrete beams. *Journal of Building Engineering*, 30, P. 101273. <https://doi.org/10.1016/j.job.2020.101273>.



- Li, X., Wu, G., Popal, M.S. and Jiang, J., 2018. Experimental and numerical study of hollow core slabs strengthened with mounted steel bars and prestressed steel wire ropes. *Construction and Building Materials*, 188, pp.456-469. <https://doi.org/10.1016/j.conbuildmat.2018.08.073>.
- Manual, A.U., 2014. Abaqus theory guide. Version 6.14. USA: Dassault Systemes Simulia Corp. <http://62.108.178.35:2080/v6.14/index.html>
- Mata Falcón, J., Bischof, P., Huber, T., Anton, A., Burger, J.J., Ranaudo, F., Jipa, A., Gebhard, L., Reiter, L., Lloret-Fritschi, E. and Van Mele, T., 2022. Digitally fabricated ribbed concrete floor slabs: a sustainable solution for construction. *RILEM Technical Letters*, 7, pp.68-78. <https://doi.org/10.21809/rilemtechlett.2022.161>.
- Michał, S. and Andrzej, W., 2015. Calibration of the CDP model parameters in Abaqus. http://www.i-asem.org/publication_conf/asem15/3.CTCS15/1w/W1D.1.AWinnicki.CAC.pdf
- Naser, M.Z., Hawileh, R.A. and Abdalla, J.A., 2019. Fiber-reinforced polymer composites in strengthening reinforced concrete structures: A critical review. *Engineering Structures*, 198, P. 109542. <https://doi.org/10.1016/j.engstruct.2019.109542>.
- Pawar, A.J., Mathew, N.S., Dhake, P.D. and Patil, Y.D., 2022. Flexural behavior of two-way voided slab. *Materials Today: Proceedings*, 65, pp. 1534–1545. <https://doi.org/10.1016/j.matpr.2022.04.500>.
- Pershakov, V., Bielyatynskiy, A. and Pylypenko, O., 2016. *Reinforced Concrete and Stone Structures*. Scholars' Press. ISBN: 978-3-639-86363-5.
- Plizzari, G. and Mindess, S., 2019. Fiber-reinforced concrete. *Developments in the Formulation and Reinforcement of Concrete*, pp. 257–287. <https://doi.org/10.1016/b978-0-08-102616-8.00011-3>.
- Pöhler, C., Bachtiar, E.V., Yan, L. and Kasal, B., 2021. Composites for structural strengthening, repair, rehabilitation, and retrofit. In *Composite Materials* (pp. 205-226). Elsevier.
- Randl, N. and Harsányi, P., 2017. Developing optimized strengthening systems for shear-deficient concrete members. *Structural Concrete*, 19(1), pp. 116–128. <https://doi.org/10.1002/suco.201600187>.
- Raza, A., Khan, Q.U.Z. and Ahmad, A., 2019. Numerical investigation of load-carrying capacity of GFRP-reinforced rectangular concrete members using CDP model in ABAQUS. *Advances in Civil Engineering*, 2019, pp. 1–21. <https://doi.org/10.1155/2019/1745341>.
- Sayhood, E., Ali, A. and Sharhan, Z., 2018. Serviceability limit state of two-way reinforced concrete slab strengthened with different techniques. *MATEC Web of Conferences*, 162, P. 04001. <https://doi.org/10.1051/matecconf/201816204001>.
- Siddiqui, H.A., Pickering, K.L. and Mucalo, M.R., 2018. A review on the use of hydroxyapatite-carbonaceous structure composites in bone replacement materials for strengthening purposes. *Materials*, 11(10). <https://doi.org/10.3390/ma11101813>.
- Taffese, W.Z. and Sistonen, E., 2017. Machine learning for durability and service-life assessment of reinforced concrete structures: Recent advances and future directions. *Automation in Construction*, 77, pp. 1–14. <https://doi.org/10.1016/j.autcon.2017.01.016>.
- Vakhshouri, V., 2017. *Comparative study of the long-term deflection of conventional and self-compacting concrete with light-weight concrete slabs* (Doctoral dissertation).
- Wang, Y.H., Tang, Q. and Nie, X., 2017. Comparative investigation on influences of concrete material constitutive models on structural behavior. *Construction and Building Materials*, 144, pp. 475–483.



<https://doi.org/10.1016/j.conbuildmat.2017.03.174>.

Wu, W., Owino, J., Al-Ostaz, A. and Cai, L. (2014) Applying Periodic Boundary Conditions in Finite Element Analysis. SIMULIA Community Conference, Providence, 707-719.

<https://www.scirp.org/reference/referencespapers?referenceid=2024207>

Yuan, W.H., Wang, H. C., Zhang, W., Dai, B.-B., Liu, K. and Wang, Y., 2021. Particle finite element method implementation for large deformation analysis using Abaqus. *Acta Geotechnica*, 16(8), pp. 2449–2462. <https://doi.org/10.1007/s11440-020-01124-2>.

Zhou, L., Zheng, Y. and Taylor, S., 2018. Finite-element investigation of the structural behavior of basalt fiber reinforced polymer (BFRP)- reinforced self-compacting concrete (SCC) decks slabs in thompson bridge. *Polymers*, 10(6), P. 678. <https://doi.org/10.3390/polym10060678>.

تحليل العناصر المحددة للبلاطات الخرسانية المسلحة المجوفة والمعززة بشرائح البوليمر المقوى بالألياف الزجاجية تحت الأحمال الثابتة والتكرارية

شهد حميد مطشر* ، عادل عبد الأمير العزاوي

قسم الهندسة المدنية، جامعة النهرين، بغداد، العراق

الخلاصة

تم صب وفحص ستة نماذج من البلاطات بإبعاد (1000*1000 ملم) مختبرياً كبلاطات بسيطة الاسناد ثنائية الاتجاه ومجوفة ثم مقارنتها مع البلاطات الصلدة المعرضة لأحمال جزئية ثابتة ومتكررة (ثلاثة تحت التحميل الثابت وثلاثة تحت التحميل المتكرر). تتكون النماذج التي تم اختبارها من بلاطة صلدة واحدة وبلاطتين مجوفتين مع المتغيرات التالية (نوع البلاطة (صلدة ومجوفة)، وجود ألياف فولاذية (0% و 1%)، وجود وعدد طبقات شرائح البوليمر المقوى بالألياف الزجاجية (GFRP). يتضمن هذا البحث دراسة نتائج فحوصات البلاطات المختبرية ومقارنتها بنتائج البرنامج النظري باستخدام برنامج العناصر المحددة (ABAQUS/ CAE FE 2019) تحت التحميل الثابت والمتكرر. تمت مناقشة عملية نمذجة المكونات الهيكلية للبلاطات التي تم اختبارها بالتفصيل، بما في ذلك إنشاء الأجزاء، خصائص المواد النموذجية، الترابط السطحي، طريقة التحميل، شروط الحدود وعمل الشبكات ثم تمت مقارنة النتائج المختبرية مع النتائج النظرية ومن ثم تمت دراسة متغيرات جديدة تؤثر على سلوك البلاطات الخرسانية المسلحة نظرياً والتي لم يتم تنفيذها في الجزء العملي من هذه الدراسة. وقد قسمت هذه النماذج إلى مجموعتين حسب طبيعة التحميل كما في العمل التجريبي. بلغت نسبة الاختلاف بين النتائج العملية والنظرية (10%) وهي درجة مقبولة كما تبين ان أنماط التشققات التي تم الحصول عليها باستخدام البرنامج النظري للنماذج التي تم فحصها تحت التحميل الثابت والمتكرر تشبه إلى حد كبير أنماط التشققات التي ظهرت على النماذج المختبرية.

الكلمات المفتاحية: العناصر المحددة، التحميل الثابت، التحميل التكراري، البلاطة المجوفة ثنائية الاتجاه، البوليمر المقوى بالألياف الزجاجية ، اباكوس.